Fourth Annual Conference of the CFD Society of Canada
June 2-6, 1996 Ottawa.

NUMERICAL SOLUTION FOR THE BOUNDARY LAYER INDUCED BY A CONICAL VORTEX

J. C. Arrese and R. Fernández-Feria
Universidad de Málaga,
E.T.S. Ingenieros Industriales, 29013 Málaga, SPAIN

Abstract. This paper addresses the problem of the interaction of inviscid vortices with solid walls perpendicular to their axis of symmetry. An interesting feature of the boundary layer equations describing this interaction for several types of axisymmetric vortices considered in the past is that they do not have self-similar solutions, in spite of the self-similar structure of the problem. We present here numerical solutions for the boundary layer equations corresponding to the interaction of a family of inviscid, but rotational, conical vortices with a disk, showing that the problem has a solution, but, as it was already known, it is not self-similar. As an important difference with previous related work, the family of inviscid vortices considered do have meridional as well as azimuthal motion, as it is the case in most of the swirling flows of practical interest.

Introduction

The structure of the flows resulting from the interaction of axisymmetric vortices with plane walls has been considered by a number of investigators because its interest in many swirling flows of technological and geophysical significance. The interaction of a rigid-body rotating flow [i.e. with velocity field $(u, v, w) \sim (0, r, 0)$ in cylindrical-polar coordinates (r, θ, z)] with a disk was first analyzed long time ago by Bödewadt [1], who found a self-similar solution to this problem. However, that flow is not strictly speaking a vortex, and the pioneering work on the subject may be considered that of Taylor [2], who analyzed the structure of the laminar boundary layer induced by a potential vortex [i.e. $(u, v, w) \sim (0, r^{-1}, 0)$] with a conical wall by using integral methods. This problem was studied by Taylor in relation to the swirl atomizer, and it was later considered by some other investigators. In particular, Rott and Lewellen [3] look for self-similar solutions to the problem, surprisingly finding that they do not exist. Burggraf et al. [4] integrated numerically the boundary layer equations and showed that although no self-similar solution exists to these equations, the boundary layer may be described by a doubly-similarity structure. This work was later generalized by Belcher et al. [5] for an inviscid vortex of the form $(u, v, w) \sim (0, r^{-n}, 0)$. These authors found numerically that self-similar solutions for the boundary layer equations exist when n is smaller than, approximately, 0.1217. For larger values of n, no self-similar solutions exist, but the boundary layer may be described again by a two-layer similarity structure.

All these works assumed that the inviscid external vortices have no meridional motion, that is $u = w = 0$. However, in most of the vortices of practical interest the meridional motion is as important as the azimuthal one, and it is therefore essential to retain it in order to study the interaction of the vortex with a plane wall. Of particular interest in the past has been the family of conical vortices with velocity field inversely proportional to r, i.e. $\Psi \sim r$ and $v \sim r^{-1}$, where Ψ is the stream function for the meridional motion, mainly because it is the only instance for which the Navier-Stokes equations for an axisymmetric swirling flow have self-similar solutions. However, it was shown by Squire [6] and by Goldshtik [7], among others (see, e.g., [8]-[9]), that, for Reynolds numbers above a critical value, these self-similar solutions cannot satisfy a no-slip velocity boundary condition at the plane if

they are allowed to be regular at the axis. For high Reynolds numbers, the structure of these flows may be described by an inviscid, but rotational, flow with velocity field inversely proportional to r, which is singular both at the axis ($r = 0$) and at the plane wall ($z = 0$) (see Appendix). This singular inviscid flow may be regularized at the axis through an axisymmetric boundary layer, whose self-similar solution was first obtained by Long [10], though it was not in relation to these conical inviscid vortices. An interesting feature of these near-axis self-similar solutions is that they exist only for a particular combination of the intensities of the swirl and the meridional motion, which in terms of the swirl parameter L, defined as the ratio between azimuthal and axial inviscid velocities near the axis, is given by $L = \sqrt{2}$ ([8],[10]-[11]). For $L \neq \sqrt{2}$ no solution exists, thus showing that for this family of swirling flows the swirl and the meridional motion are necessarily bounded, as it is the case in many swirling flows of practical interest. Near the plane, the boundary layer equations regularizing the singular inviscid behavior have also a self-similar structure (see below). However, it was shown in [12] that no self-similar solution exists with the boundary condition of zero velocity at the wall (although other boundary conditions may be allowed), as it was already known from the full Navier-Stokes equations for Reynolds numbers above a critical value (e.g. [8]-[9]). We shall present in this work the numerical solution to these boundary layer equations assuming that the plane wall is a finite disk perpendicular to the axis of the vortex. These solutions may be of interest for several reasons. First, to show that the problem of the interaction of a conical vortex of the type r^{-1} with a plane for high Reynolds numbers has a solution, though it is not self-similar. This solution corresponds to a relatively simple and interesting example of a three-dimensional boundary layer for a swirling flow on a plane where the inviscid meridional motion is as important as the azimuthal one. Also, the knowledge of the terminal structure of the boundary layer at the core would provide an initial profile for studying near-axis swirling flows of technological as well as geophysical (atmospherical) interest. Finally, and perhaps most important, the numerical solution will be a guide to look for approximate asymptotic solutions, which are of a more practical interest, and are given elsewhere.

Governing equations

Our objective is to solve numerically the axisymmetric boundary layer equations for an incompressible fluid of density ρ and kinematic viscosity ν, which in cylindrical polar coordinates may be written as

$$\frac{\partial(ur)}{\partial r} + \frac{\partial(wr)}{\partial z} = 0, \tag{1}$$

$$u\frac{\partial u}{\partial r} + w\frac{\partial u}{\partial z} - \frac{v^2}{r} = -\frac{\partial p/\rho}{\partial r} + \nu\frac{\partial^2 u}{\partial z^2}, \tag{2}$$

$$u\frac{\partial v}{\partial r} + w\frac{\partial v}{\partial z} + \frac{uv}{r} = \nu\frac{\partial^2 v}{\partial z^2}, \tag{3}$$

where p is the pressure, on a flat disk of radius R perpendicular to the axis of symmetry z. The boundary layer is induced by the conical inviscid vortex given in the Appendix. In particular, the inviscid swirling flow outside the boundary layer is given by the asymptotic expressions (45)-(48) in that Appendix, which yield a singular radial velocity at $z = 0$. Equations (45)-(48) may be written as ($z/r \to 0$):

$$\Psi \sim K(rz)^{1/2}(1 - \frac{1}{2}\frac{z}{r} + O(\frac{z^2}{r^2})), \tag{4}$$

$$v \sim \frac{K}{r}, \tag{5}$$

$$\frac{p}{\rho} \sim -\frac{K^2}{2r^2}(\frac{z}{r} + O(\frac{z^2}{r^2})). \tag{6}$$

where Ψ is the stream function for the meridional motion, through which u and w are given by

$$rw = \partial\Psi/\partial r, \quad ru = -\partial\Psi/\partial z. \tag{7}$$

The order of magnitude of the boundary layer thickness, δ, may be determined, as usual, by comparing the viscous and convective terms in (2)-(3) when the external flow (4)-(5) is used. In terms of the Reynolds number based on the circulation K and ν, one has

$$\frac{\delta}{R} \sim Re^{-\frac{2}{3}}, \quad Re \equiv \frac{K}{\nu} \gg 1. \tag{8}$$

It must be remembered from the Appendix that the intensity of the meridional motion is of the same order as the swirl intensity, so that the Reynolds number (8) characterizes both motions. According to (8) and (4)-(6), it is convenient to define the dimensionless independent and dependent variables, (ξ, η) and (F, G), respectively, as

$$\xi \equiv \frac{r}{R}, \quad \eta \equiv \frac{z}{\delta(r)}, \quad \delta(r) \equiv Re^{-\frac{2}{3}} R\xi, \quad (9)$$

$$\Psi \equiv \nu R\xi Re^{2/3} F(\xi, \eta), \quad (10)$$

$$v \equiv \nu \frac{Re}{R\xi} G(\xi, \eta), \quad (11)$$

through which equations (2)-(3) become (Eq. (1) is satisfied identically)

$$F_{\eta\eta\eta} - F_\eta^2 - F F_{\eta\eta} = \xi[F_\xi F_{\eta\eta} - F_\eta F_{\eta\xi}]$$

$$- Re^{-\frac{2}{3}} g^2 - \frac{3}{2} Re^{-\frac{4}{3}} \eta, \quad (12)$$

$$G_{\eta\eta} - F G_\eta = \xi[F_\xi G_\eta - F_\eta G_\xi]. \quad (13)$$

To write these equations, use has been made of the definitions (7) of u and w in terms of F,

$$u = -\nu \frac{Re^{4/3}}{R\xi} F_\eta, \quad (14)$$

$$w = \nu \frac{Re^{2/3}}{R\xi} [F + \xi F_\xi - \eta F_\eta], \quad (15)$$

where the subscripts η and ξ mean differentiation with respect to these variables. The terms proportional to negative powers of Re in the right hand side of (12), which come from the centrifugal and pressure forces in (2), are very small, and may be neglected at the lowest order of the boundary layer approximation given here (we shall solve the formal limit $Re \to \infty$). Thus, equation (12) becomes decoupled from (13) and may be integrated separately.

The boundary conditions are the following: At the disk edge ($\xi = 1$ and any η), and outside the boundary layer ($\eta \to \infty$ and any ξ), the flow is given by (4)-(6), which in terms of the new dimensionless variables may be written as

$$F = \eta^{\frac{1}{2}} (1 - \frac{1}{2} Re^{-\frac{2}{3}} \eta + O(Re^{-\frac{4}{3}} \eta^2)), \quad (16)$$

$$G = 1. \quad (17)$$

Again, we shall neglect terms proportional to negative powers of Re in (16). On the disk ($\eta = 0$ and any ξ), the velocity is zero,

$$F = F_\eta = G = 0. \quad (18)$$

It must be noted here that in the definition (9) of the dimensionless variable η we have used the local boundary layer thickness, $\delta(r)$, instead of its value at the disk edge (19). The reason is that for $\xi \to 0$, the right hand sides of equations (12)-(13) become null, and the problem (12)-(13) with (16)-(18) has a self-similar structure. The problem is thus reduced to solving a decoupled system of ordinary differential equations for $F(\eta)$ and $G(\eta)$. However, it is shown in [12], where the solution to Eq. (12) in this limit is further reduced to the integration of a first order, nonlinear differential equation, that this self-similar problem has no solution. More precisely, it is shown that in the corresponding phase-plane of Eq. (12), there are no trajectories going from the singular point corresponding to (16)-(17) to that of (18). As mentioned in the Introduction, this is a common feature of other boundary layers induced by vortices, and it is the reason why we undertake here the numerical integration of (12)-(13) with (16)-(18) retaining the dependence of F and G on ξ.

Numerical procedure

To solve numerically the above problem we use a finite difference method. Since the system of equations (1)-(3) is parabolic, and provided that $u \leq 0$ ($F_\eta \geq 0$, as it will be the case in the reported computations), one may start at the edge of the disk, $\xi = 1$, and proceeds towards the axis $\xi = 0$. Since the numerical integration will start at $\xi = 1$, it is convenient to re-scale the variables (9)-(11) to account for the singularity there. It must be noted that the variables (9)-(11) already account for the (*similarity*) behavior as $\xi \to 0$. However, these variables are not very appropriate near $\xi = 1$ because, among other things, the boundary layer thickness at $\xi = 1$ is zero instead of that given by (8). The appropriate scaling factors near $\xi = 1$ are obtained from (2)-(3) taking into account (4)-(5) with $r \simeq R$. One obtains:

$$\delta \sim R(1-\xi)^{\frac{2}{3}}, \quad F \sim (1-\xi)^{\frac{1}{3}}, \quad G \sim 1. \quad (19)$$

On the other hand, from a numerical point of view, it is more convenient to use the meridional velocity components instead of the stream function for the integration; i.e. we shall use the original set of equations (1)-(3) instead of (12)-(13). The new dimensionless variables which take into account the scaling factor near $\xi = 1$ are:

$$\gamma = \frac{\eta}{(1-\xi)^{\frac{2}{3}}}, \tag{20}$$

$$f = 2(1-\xi)^{\frac{1}{3}} F_\eta = -2\frac{(1-\xi)^{\frac{1}{3}}\delta^2(r)}{\nu r}\, u, \tag{21}$$

$$h = 2\frac{F + \xi F_\xi - \eta F_\eta}{(1-\xi)^{\frac{1}{3}}} = 2\frac{\delta(r)}{\nu(1-\xi)^{\frac{1}{3}}}\, w, \tag{22}$$

$$g = G = \frac{\delta^{3/2}(r)}{\nu r^{1/2}}\, v. \tag{23}$$

Finally, we re-define the independent variable

$$l = -\ln(\xi) \tag{24}$$

in order to numerically reach the axis *more slowly*. Introducing (20)-(24) into (1)-(3) we arrive at:

$$\chi_2(l) h_\gamma = [\chi_2(l) - \chi_3(l)] f + \chi_2(l)\gamma f_\gamma - \chi_3(l) f_l = 0, \tag{25}$$

$$2f_{\gamma\gamma} + \chi_1(l) f^2 + [\chi_2(l)\gamma f - \chi_3(l) h] f_\gamma - \chi_3(l) f f_l = 0, \tag{26}$$

$$2g_{\gamma\gamma} + [\chi_2(l)\gamma f - \chi_3(l) h] g_\gamma - \chi_3(l) f g_l = 0, \tag{27}$$

where

$$\chi_1(l) = -1 + \frac{4}{3}e^{-l}, \quad \chi_2(l) = -1 + \frac{5}{3}e^{-l},$$

$$\chi_3(l) = 1 - e^{-l}.$$

The boundary conditions (16)-(18) become

$$f = g = h \quad at \quad \gamma = 0, \tag{28}$$

$$f(l,\gamma) = \gamma^{-\frac{1}{2}}, \quad h(l,\gamma) = \gamma^{\frac{1}{2}}, \quad g(l,\gamma) = 1, \quad at \quad l = 0 \quad or \quad \gamma \to \infty. \tag{29}$$

Although we shall use this set of variables (f,g,h) and (l,γ) to perform the numerical computations, the results will be given in terms of (F,G) and (ξ,η) (see next section). The conversion between both sets of variables is made through (20)-(24).

The above set of non-linear equations is solved iteratively at each station starting from the disk edge $l = 0$. To this end, for an arbitrary function $q(l_i, \gamma_j)$, we define the symbols q_j, q'_j, $\bar{q}_j$ as follows:

$$q_j = q(l_i, \gamma_j), \tag{30}$$

$$q'_j = q(l_{i+1}, \gamma_j), \quad \bar{q}_j = \frac{1}{2}(q_j + q'_j), \tag{31}$$

where $l_{i+1} = l_i + \Delta l$, and $\gamma_{j\pm1} = \gamma_j \pm \Delta\gamma$. Derivatives are defined using central differences:

$$\frac{\partial q}{\partial l} = \frac{q'_j - q_j}{\Delta l}, \quad \frac{\partial q}{\partial \gamma} = \frac{\bar{q}_{j+1} - \bar{q}_{j-1}}{2\Delta\gamma}, \tag{32}$$

etc. Thus, the momentum equations (26)-(27) may be expressed in matrix notation as

$$\{A\}\{f'\} = \{b_1\}, \quad \{A\}\{g'\} = \{b_2\}, \tag{33}$$

where

$$\{A\} = \begin{pmatrix} y_1 & z_1 & 0 & 0 & \dots & 0 \\ x_2 & y_2 & z_2 & 0 & \dots & 0 \\ 0 & x_3 & y_3 & z_3 & \dots & 0 \\ 0 & 0 & x_4 & y_4 & \dots & 0 \\ \cdot & \cdot & \cdot & \cdot & \dots & \cdot \\ \cdot & \cdot & \cdot & \cdot & \dots & \cdot \\ 0 & 0 & 0 & 0 & \dots & y_n \end{pmatrix}, \tag{34}$$

and where

$$x_k = \frac{2}{(\Delta\gamma)^2} - \frac{1}{2\Delta\gamma}[\chi_2(\bar{l})\gamma_k \bar{f}_k - \chi_3(\bar{l})\bar{h}_k],$$

$$y_k = -\frac{4}{(\Delta\gamma)^2} - \frac{2\chi_3(\bar{l})}{\Delta l}\bar{f}_k, \tag{35}$$

$$z_k = \frac{2}{(\Delta\gamma)^2} + \frac{1}{2\Delta\gamma}[\chi_2(\bar{l})\gamma_k \bar{f}_k - \chi_3(\bar{l})\bar{h}_k].$$

Since the problem is nonlinear, the column vectors $\{b_1\}$ and $\{b_2\}$ depend not only on the flow properties at the previous l_i-station, but also on the unknown properties at the present

l_{i+1}-station. Therefore, one must solve the problem iteratively. In each iteration, we use a high accuracy Gaussian elimination method from the IMSL Subroutine Library to solve the linear equations (32). The value of h is computed at each iteration via the continuity equation (24) by using a numerical quadrature also from the IMSL Library.

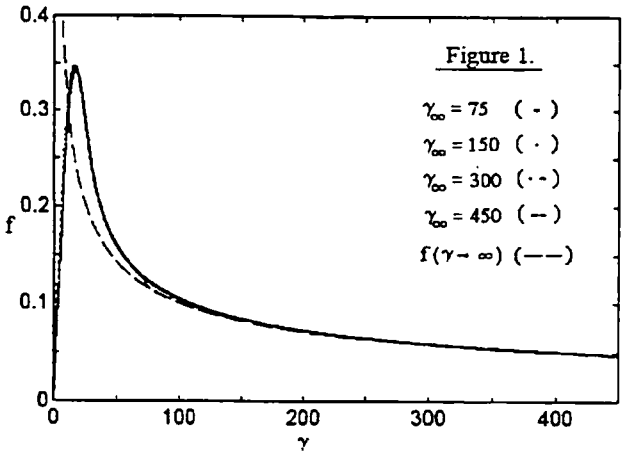

The accuracy of the results and the computation time depend on the step sizes, Δl and $\Delta\gamma$, and, since γ varies between 0 and ∞, also on the truncation value of γ, γ_∞, where the boundary condition (29) is imposed. Figure 1 shows the solution f as a function of γ for $l = 0.6931$ ($\xi = 0.5$) and different values of γ_∞ (these calculations have been made with $\Delta l = 0.005$ and $\Delta\gamma = 0.2$). It is observed that for all the values of γ_∞ used the solution is practically the same (it is difficult to recognize the different curves in figure 1), except in a very small region near $\gamma = \gamma_\infty$. Therefore, the truncation value γ_∞ is not very critical, provided that it is, of course, much larger than unity. We have used $\gamma_\infty = 300$ in all the reported computation given in the next section. To choose $\Delta\gamma$ and Δl, we have carried out different simulations for different values of these increments.

$\Delta\gamma$	l=0.5	l=1.0
1.0	(15.30 , 0.350)	(33.10 , 0.200)
0.2	(18.05 , 0.370)	(35.90 , 0.219)
0.1	(18.10 , 0.371)	(36.00 , 0.220)
0.05	(18.12 , 0.371)	(36.10 , 0.221)

Table 1. Description in the text.

Table 1 shows the effect of the variation of $\Delta\gamma$. In paricular, we show there (γ_0, f_0), where f_0 is the maximum value of f and γ_0 its position (see, e.g., figure 1), for two values of l and different $\Delta\gamma$. We have used (γ_0, f_0) to characterize the accuracy because it is the point where the differences are, by far, the greatest. From this table it is clear that a value $\Delta\gamma$ of the order of 10^{-1} is appropriate. We have used $\Delta\gamma = 0.15$ for all the computations given in the next section. In relation to Δl, one should take a compromise between accuracy and computation time: As Δl decreases the computation time increases very fast because more steps are needed to reach a given value of l (although, the number of iterations needed at each l-station for convergence decreases). Thus, if one takes a very small value of Δl the amount of time to reach the vicinity of the axis ($l \to \infty$) is enormous. We have used $\Delta l = 5 \cdot 10^{-3}$ in all the computations except in the first step, for which the value $\Delta l = 5 \cdot 10^{-5}$ is used in order to reduce the number of iterations. In general, the computations converged rapidly at each l-station, requiring roughly between 20 and 25 iterations to pass a tolerance of 10^{-6} (except at the first station, where about 50 iterations were needed).

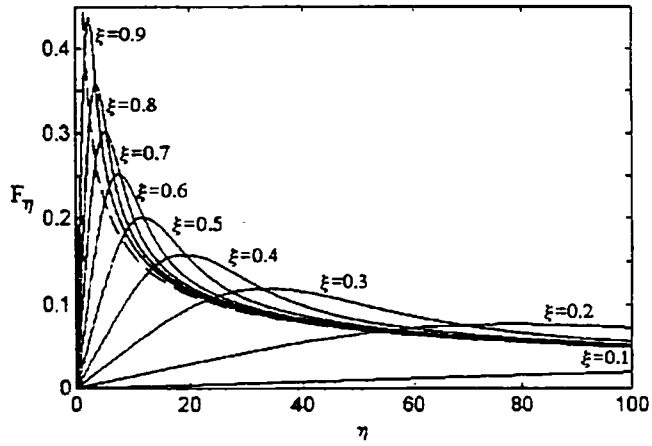

Figure 2: Dimensionless radial velocity profiles, $F_\eta = -R\xi u/(\nu Re^{4/3})$, as a function of η for $\xi = 0.1, 0.2, ..., 0.9$. The dashed line corresponds to the boundary condition at $\eta \to \infty$, $F_\eta \to 1/(2\sqrt{\eta})$.

Results and discussion

All the results presented here are in the variables (ξ, η) and (F,G). Figure 2 shows F_η (proportional to the radial velocity, see (14)) as a function of η for different values of ξ. The maximum value of F_η, $u_0(\xi)$, and its position, $\eta_0(\xi)$, are plotted in figures 5 and 6, respectively. The dimensionless azimuthal velocity G and the stream function F are plotted as a function of η for several values of ξ in figures 3 and 4, respectively. The function F has been calculated from f via equation (21) by a simple numerical quadrature. Finally, figures 5 and 6 depict also the magnitudes $F_{\eta\eta}(\eta = 0)$ and $G_\eta(\eta = 0)$ as a function of ξ, which are proportional to the radial and azimuthal shear stresses at the surface, respectively, and their ratio $F_{\eta\eta}(\eta = 0)/G_\eta^2(\eta = 0)$, of interest to characterize the structure of the solution near the plane.

Several comments may be said from these results. First, it is shown that, indeed, the problem has a solution, though it is clear that the solution is not self-similar, since the functions F and G depend strongly on ξ, as well as on η. However, a two-layer structure of the solution may be envisaged, mainly from figures 2 and 3 for the radial and azimuthal velocity profiles: there is an outer region where the solution differs only slightly from the outer inviscid flow, and an inner region where F_η has a pronounced maximun and G reaches its outer value quite rapidly. The thicknesses of each of these two layers depend on ξ. We can estimate the thickness of the interior layer from the value $\eta_0(\xi)$, or position of the maximum of the radial velocity F_η (figure 6). For small ξ, figure 6 tells us that this thickness varies as ξ^{-2}. Also from figure 6, it is observed that the ratio $F_{\eta\eta}(\eta = 0)/G_\eta^2(\eta = 0)$ varies as ξ^{-1} for small ξ, which tell us that F is of that order in the interior layer. These two scaling factors are useful to describe the solution in the interior layer. Indeed, using the present numerical results we show elsewhere that, for small ξ, the structure of these two layers may be described in terms of asymptotic similarity solutions.

Appendix: Inviscid conical flow

In this appendix we consider the solution to the steady Euler equations for an incompressible fluid

$$\nabla \cdot \mathrm{u} = 0, \quad \rho \mathrm{u} \cdot \nabla \mathrm{u} + \nabla p = 0, \tag{36}$$

of the form:

$$\Psi = \Upsilon(y) r, \quad y \equiv r/z, \tag{37}$$

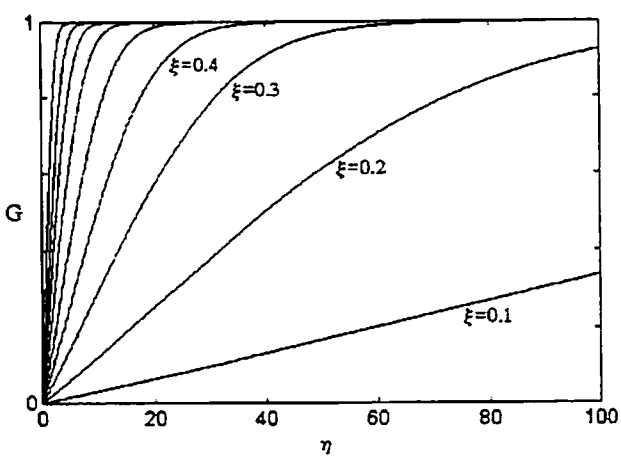

Figure 3: Dimensionless azimuthal velocity, $G = R\xi v/(\nu Re)$, as a function of η for $\xi = 0.1, 0.2, ..., 0.9$. The boundary condition as $\eta \to \infty$ is $G = 1$.

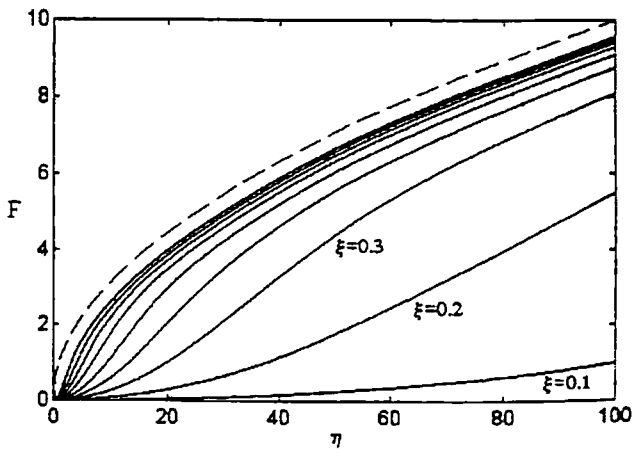

Figure 4: Dimensionless stream function, $F = \Psi/(\nu R\xi Re^{2/3})$, as a function of η for $\xi = 0.1, 0.2. ..., 0.9$. The dashed line corresponds to the boundary condition as $\eta \to \infty$, $F \to \sqrt{\eta}$.

$$v = \Omega(y) r^{-1}, \tag{38}$$

$$p/\rho = \Pi(y) r^{-2}. \tag{39}$$

This is a particular case of the more general family of inviscid conical vortices considered in [12] (case m=1), for which the resulting equations may be solved in a closed form:

$$\Upsilon(y) = \frac{4K}{L^4} \frac{[\sqrt{1+y^2} - 1]^{\frac{1}{2}}}{y}, \tag{40}$$

$$\Omega = K, \tag{41}$$

$$2\Pi = (\frac{K}{L})^4 \Upsilon^{-2} - (\Upsilon + y\Upsilon')^2 - y^4 \Upsilon'^2 - \Omega^2, \tag{42}$$

where K and L are arbitrary constants. $K/2\pi$ is the circulation of the vortex, while L is the swirl parameter, or ratio between the azimuthal and axial velocity components near the axis:

$$L = \left(\frac{v}{w}\right)_{y \to 0}. \tag{43}$$

At the axis ($y = 0$), expressions (40)-(42) yield a singular inviscid flow field. As mentioned in the Introduction, the regularization of this singular flow through a near-axis boundary layer fixes $L = \sqrt{2}$ [10]-[11]. At the plane ($y \to \infty$), (40) behaves as:

$$\Upsilon(y) \sim K y^{-\frac{1}{2}} (1 - \frac{1}{2} y^{-1} + O(y^{-2})) \tag{44}$$

which, again, yields a singular velocity field,

$$w \sim \frac{1}{2} K r^{-\frac{3}{2}} z^{\frac{1}{2}} (1 + O(\frac{z}{r})), \tag{45}$$

$$u \sim -\frac{1}{2} K (rz)^{-\frac{1}{2}} (1 + O(\frac{z}{r})), \tag{46}$$

$$v \sim K r^{-1}, \tag{47}$$

$$\frac{p}{\rho} \sim -\frac{K^2}{2} \frac{z}{r^3} (1 + O(\frac{z}{r})), \tag{48}$$

and must be regularized through a near axis viscous boundary layer, as done in the main text.

References

[1] U.T. Bödewadt, "Die Drehströmung über festem Grunde", ZAMM, Vol. 20, pp. 241-253, 1940.

[2] G.I. Taylor, "The boundary layer in the converging nozzle of a swirl atomizer", Quart. J. Mech. Appl. Math., Vol. 3, pp. 129-139, 1950.

[3] N. Rott and W.S. Lewellen, "Boundary layers and their interactions in rotating flows", Progress in Aeronautical Science, ed. by D. Kuchemann. Pergamon, Vol. 7, pp. 111, 1966.

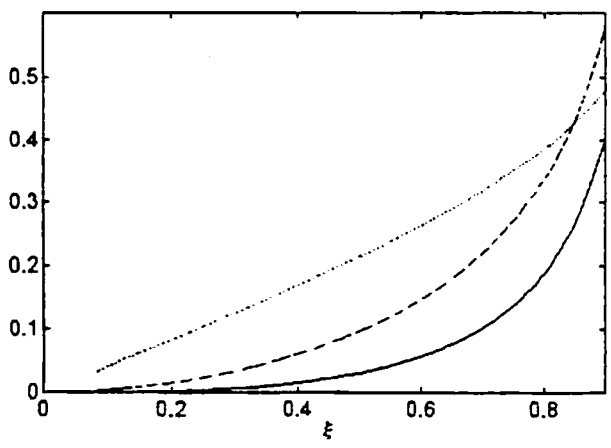

Figure 5: $F_{\eta\eta}(\eta = 0)$ (continuous line); $G_\eta(\eta = 0)$ (dashed line) and u_0, or maximum of F_η (dotted line), as function of ξ.

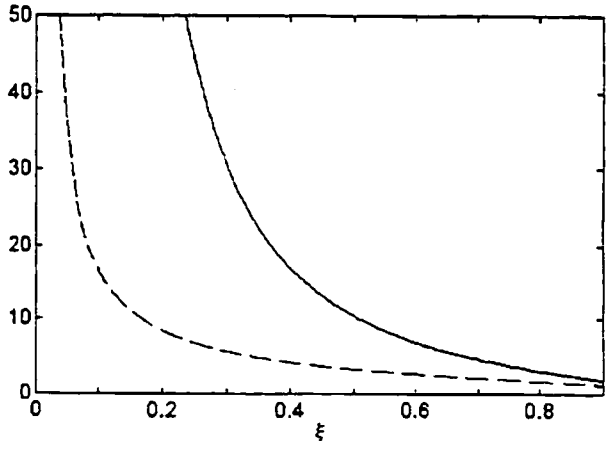

Figure 6: $F_{\eta\eta}(\eta = 0)/G_\eta^2(\eta = 0)$ (continuous line), and η_0 (dashed line) as a function of ξ.

[4] O.R. Burggraf, K. Stewartson and R.J. Belcher, "Boundary layer induced by a potential vortex", Physical Fluids, Vol. 14, pp. 1821-1833, 1971.

[5] R.J. Belcher, O.R. Burggraf and K. Stewartson, "On generalized-vortex boundary layers", J. Fluid Mech., Vol. 52, pp. 753-780, 1972.

[6] H.B. Squire, "Some viscous fluid flow problems, I. Jet emerging from a hole in a plane wall", Phil. Mag., Vol. 43, pp. 942-945, 1952.

[7] M.A. Goldshtik, "A paradoxical solution of the Navier-Stokes equations", Appl. Mat. Mech. (Sov.), Vol. 24, pp. 610-621, 1960.

[8] M.A. Goldshtik and V.M. Shtern, "Collapse in conical viscous flows", J. Fluid Mech., Vol 218, pp. 483-508, 1990.

[9] C. Sozou, "On solutions relating to conical vortices over a plane wall", J. Fluid Mech., Vol. 244, pp. 633, 1992.

[10] R.L. Long, "A vortex in an infinite viscous fluid", J. Fluid Mech., Vol. 218, pp. 611-625, 1961.

[11] R. Fernández-Feria, J. Fernández de la Mora and A. Barrero, "Solution breakdown in a family of self-similar nearly inviscid axisymetric vortices", J. Fluid Mech., Vol. 305, pp. 77, 1995.

[12] R. Fernández-Feria, J. Fernández de la Mora and A. Barrero, "Conically similar swirling flows at high Reynolds numbers. Part 1. One-cell solutions", SIAM J. Appl. Math. (submitted).